Two-subband quantum Hall effect in parabolic quantum wells

C. Ellenberger,[1] B. Simovič,[1] R. Leturcq,[1] T. Ihn,[1] S. E. Ulloa,[1,*] K. Ensslin,[1] D. C. Driscoll,[2] and A. C. Gossard[2]

[1]*Solid State Physics Laboratory, ETH Zurich, 8093 Zurich, Switzerland*
[2]*Materials Department, University of California, Santa Barbara, California 93106, USA*

The low-temperature magnetoresistance of parabolic quantum wells displays pronounced minima between integer filling factors. Concomitantly the Hall effect exhibits overshoots and plateaulike features next to well-defined ordinary quantum Hall plateaus. These effects set in with the occupation of the second subband. We discuss our observations in the context of single-particle Landau fan charts of a two-subband system empirically extended by a density dependent subband separation and an enhanced spin splitting g^*.

PACS number(s): 73.43.−f

At low temperatures a two-dimensional electron gas subject to a perpendicular magnetic field gives rise to the integer quantum Hall effect.[1] The Hall effect takes on quantized values $\rho_{xy}=h/e^2\nu$ around magnetic fields $B=N_s h/e\nu$, with the integer filling factor ν counting the number of occupied Landau levels and N_s being the carrier density. In these plateau regions of ρ_{xy} the magnetoresistance ρ_{xx} is exponentially suppressed. Each Landau level is described by a Landau level quantum number $n=0,1,2,\ldots$, a spin quantum number $s=\pm 1/2$ and a subband or well index i if several subbands in a quantum well are occupied or a double well system is investigated.

Several previous experiments investigated electronic transport in systems with two occupied orbital states focusing on interlayer charge transfer at various filling factors[2] or the behavior of skyrmions in bilayer quantum Hall states.[3] Also additional minima in the magnetotransport of double layer systems as well as hysteretic behavior was observed[4,5] which was attributed to more subtle interaction effects.[6,7] For a review see Ref. 8. In a pioneering paper Muraki *et al.*[9] observed a complex structure in ρ_{xx} as well as in ρ_{xy} in a symmetric quantum well where states with different orbital indices cross at the Fermi level. The authors explain their observations in terms of charge excitations in easy-axis and easy-plane quantum Hall ferromagnets. Davies *et al.*[10] have reported measurements on a narrow-barrier double-quantum well, where the occupation of a second subband leads to additional maxima and minima in ρ_{xx} *between* integer filling factors, accompanied by overshoots and undershoots of ρ_{xy}. Zhang *et al.*[11] presented comparable data in a quantum well system with two occupied subbands. Here we report similar results obtained on *parabolic* quantum wells in which the subband occupation can be controlled by front and back gate voltages. We find that the observed phenomena can be qualitatively accounted for using an effective single-particle model where interaction effects beyond the mean field Hartree and exchange interactions are neglected.

Our samples are 100 nm wide parabolic $Al_xGa_{1-x}As$ quantum wells with the Al content varying from $x=0.4$ at the edges to $x=0$ in the center of the parabola. Hall bars with Ohmic contacts were fabricated. A Schottky front gate and a back gate[12] allows one to tune the electron sheet density N_s and with it the number of occupied subbands. At a temperature of 100 mK and gate voltages set to zero the electron mobility is 16 m^2/V s and $N_s=3.3\times10^{15}$ m^{-2}. While we

have investigated many similar samples in the past[12–16] only one (Figs. 8 and 9 of Ref. 14) showed features which might be precursors of the pronounced structures presented here. The only difference of the present compared to previous samples is the slightly higher mobility (10–20%). Data was taken by two different experimentalists over a period of two years on three different samples from the same wafer with Hall bars of different sizes. All results are comparable and highly reproducible. In the following we show coherent data from one sample.

Figure 1 shows typical experimental ρ_{xx} and ρ_{xy} traces when the second subband is populated. At magnetic fields $B<1$ T Shubnikov–de Haas (SdH) oscillations are observed. The fast oscillation period is related to the lower subband density $N_s^{(1)}=3.69\times10^{15}$ m^{-2} and the slow amplitude modulation to the upper subband density $N_s^{(2)}=1.48\times10^{14}$ m^{-2}. At $B>4$ T standard SdH oscillations as well as quantum Hall (QH) plateaus occur corresponding to the total carrier density $N_s^{tot}=N_s^{(1)}+N_s^{(2)}=3.84\times10^{15}$ m^{-2}. The unusual behavior at 2 T$<B<4$ T is enlarged in the inset of Fig. 1. An additional minimum occurs in ρ_{xx} between filling factors $\nu=4$ and 5, accompanied by an oscillatory feature in ρ_{xy} (arrow in the inset). These unexpected experimental observations are the
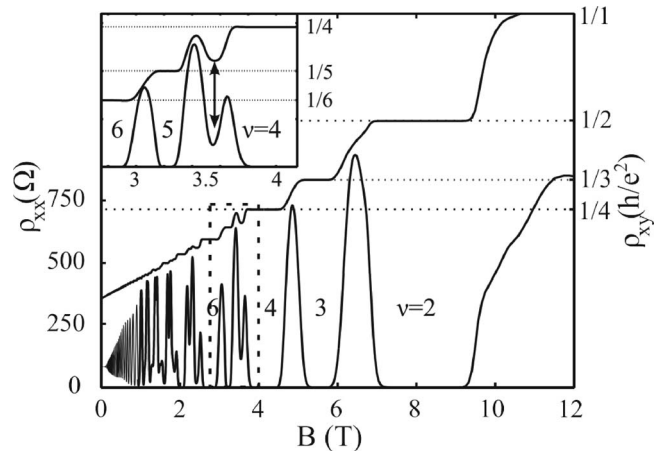

FIG. 1. Magnetoresistance ρ_{xx} (left hand scale, lower curve) and Hall resistance ρ_{xy} (right hand scale, upper curve) measured at $T=100$ mK. The horizontal lines indicate the position of the theoretically expected Hall plateaus. The inset in the upper left corner shows the same data but expanded in the regime of interest.
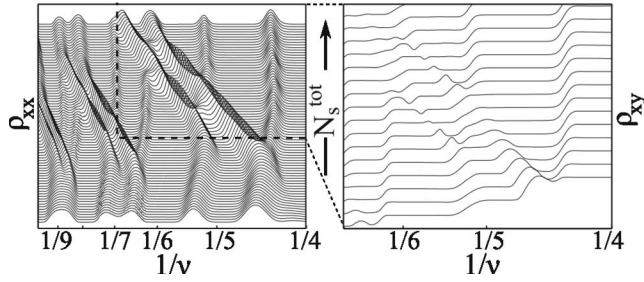
FIG. 2. Magnetoresistance ρ_{xx} (left) and Hall resistance ρ_{xy} (right) at $T=100$ mK as a function of the inverse filling factor $1/\nu=eB/hN_s^{\text{tot}}$. Curves for different carrier densities N_s^{tot} are vertically offset for clarity. The carrier density N_s^{tot} was tuned between 3.4×10^{15} and 4.85×10^{15} m^{-2} (left) and between 3.77×10^{15} and 4.85×10^{15} m^{-2} (right). The parameter range of the right figure is indicated by the dashed lines in the left figure.

focus of this paper and will be presented in more detail in the following.

Figure 2 shows the magnetoresistance (left) and Hall resistance (right) for a data set where the carrier density N_s^{tot} as determined from the classical low-field Hall effect was tuned using the front gate. By plotting the data as a function of $1/\nu$ features related to the same filling factor line up vertically. The magnetoresistance maximum between $\nu=4$ and 5 splits as a function of increasing N_s, crosses the $\nu=5$ and 6 valleys and joins the maximum between $\nu=6$ and 7. Similarly the maximum between $\nu=5$ and 6 moves into the maximum between $\nu=7$ and 8. Weaker features with qualitatively similar behavior are observed for the lower two sets of inverse filling factors. As one follows, e.g., the $\nu=5$ minimum, for low carrier densities (curves on the bottom of the figure) a single minimum is observed. As the carrier density is increased a double minimum feature (i.e., an additional maximum) occurs which then returns to a single minimum feature once the crossing regime is passed.

The Hall effect ρ_{xy} shown on the right of Fig. 2 shows an oscillatory feature between two quantum Hall plateaus if ρ_{xx} shows an additional maximum. In general the derivative $d\rho_{xy}/dB$ always behaves very similarly to ρ_{xx}.[17] Therefore we will restrict our discussion in the following to the behavior of ρ_{xx}.

In order to define the parameter space more precisely we present low-field ρ_{xx} data in a grey scale plot in Fig. 3 as a function of filling factor. The vertical axes corresponds to the electron density N_s^{Hall} as determined from the classical Hall effect at magnetic fields below 0.5 T, tuned with a front gate voltage. For densities below $N_s^{\text{Hall}} < N_s^{\text{thresh}} \approx 3.5\times10^{15}$ m^{-2} the ρ_{xx} minima corresponding to bright lines in the grey scale plot run vertically. This corresponds to the situation where one subband is occupied and the density $N_s^{(1)}$ obtained from SdH oscillations agrees with the Hall density N_s^{Hall} within measurement accuracy. At the threshold density of $N_s^{\text{thresh}} \approx 3.5\times10^{15}$ m^{-2} the second subband becomes populated and therefore the total density measured via the Hall effect increases more strongly than $N_s^{(1)}$ (see upper inset). This manifests itself by a sudden bending of the bright lines indicated, e.g., by the dashed line following filling factor $\nu_1=24$ for the lower subband. This way the carrier densities
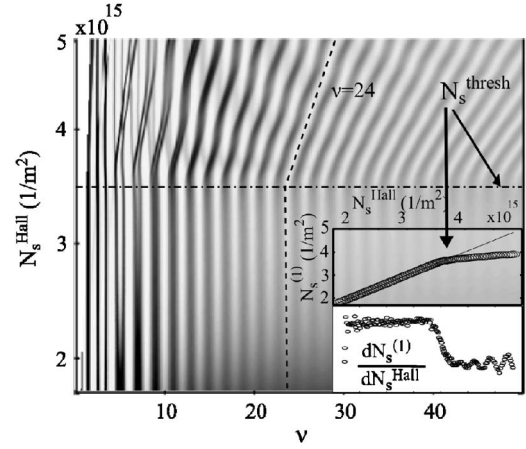

FIG. 3. Greyscale image of the magnetoresistance ρ_{xx} versus filling factor calculated from the density extracted from the low-field Hall resistance and the applied magnetic field. The horizontal dash-dotted line marks the population onset of the second subband. The vertical dashed line follows the behavior of filling factor for the lower subband $\nu_1=24$. This dashed line is converted to a density and plotted in the top inset versus the Hall density. The lower inset shows the derivative $dN_s^{(1)}/dN_s^{\text{Hall}}$ of the data in the upper inset highlighting the threshold density and revealing additional oscillations in $N_s^{(1)}$.

of both subbands $N_s^{(1)}$ and $N_s^{(2)}=N_s^{\text{tot}}-N_s^{(1)}=N_s^{\text{Hall}}-N_s^{(1)}$ can be determined.[14,15] The solid line in the upper inset of Fig. 3 shows the relation $N_s^{\text{tot}}=N_s^{\text{Hall}}$. The dashed line in the main figure related to $\nu_1=24$ is plotted by circles and basically follows the solid line until the second subband becomes populated for $N_s^{\text{tot}} \lesssim N_s^{\text{thresh}}$. For low enough magnetic fields, where the cyclotron energy $\hbar\omega_c$ is much smaller than the Fermi energy E_F, magnetic field induced redistribution of charges between the two subbands is small.[14] Only weak oscillations can be detected in $dN_s^{(1)}/dN_s^{\text{Hall}}$ (lower inset of Fig. 3) which become more pronounced for higher magnetic fields. We also note that N_s^{Hall} as a function of front gate voltage increases its slope at N_s^{thresh} due to the increased density of states at the Fermi energy.

In order to check the influence of the confining potential we have measured the magnetoresistance ρ_{xx} for different values of the back gate voltage while tuning the carrier density via the front gate. A particular example is shown in Fig. 4(e). All these measurements show the same dominant ring-like features at the same density values. We conclude that it is the density which is responsible for the onset of the additional features in the magnetoresistance.

Data has also been taken for magnetic fields tilted with respect to the sample normal. Figure 5 displays a greyscale plot of the magnetoresistance as a function of tilt angle and perpendicular magnetic field for fixed total carrier density. In contrast to previous observations done before,[18] we see a shift of the additional peak (dark central line between the ρ_{xx} minima labeled with filling factors 4 and 6) towards higher magnetic fields when exposed to an increasing inplane magnetic field.

If the diamagnetic shift resulting from the in-plane field component is considered the data look again very similar to
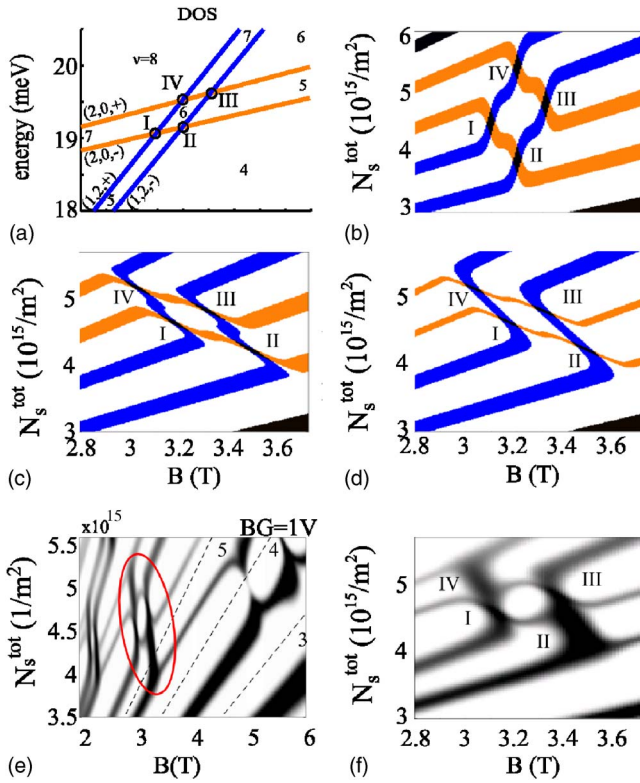
FIG. 4. (Color online) (a) Two spin-split Landau levels belonging to different subbands cross. (b) The same Landau levels as in (a) plotted in the N_s^{tot}-B plane. (c) Crossing of the same Landau levels assuming a density dependent subband spacing ΔE. (d) Crossing of the Landau levels as in (c) but allowing for different Landau-level broadenings Γ_1 and Γ_2 in the two subbands. (e) Measured ρ_{xx} in the N_s^{tot}-B plane. The encircled region in magnified in (f). Corresponding crossing points I-IV are labeled consistently in (a)-(f).

Fig. 4(e). For very high in-plane magnetic fields $B_{in-plane} > 4T$ the threshold density N_s^{thresh}, where the second subband becomes populated can no longer be reached without significant parallel conduction in the doping layer. From the available data we have no indication that spin effects, which are expected to become more dominant for large in-plane fields, become more pronounced.
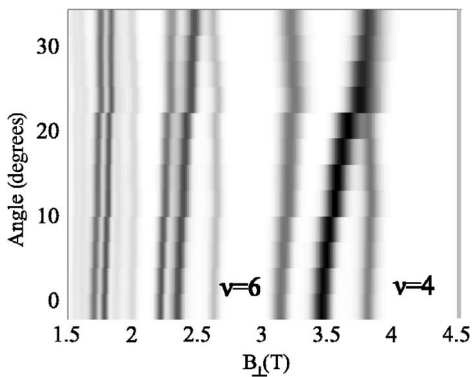

FIG. 5. Grayscale plot of magnetoresistance ρ_{xx} as a function of perpendicular magnetic field and rotation angle at a density of $N_s^{tot}=3.89\times10^{15}$ m^{-2}.

Temperature dependent experiments show that the additional minima disappear at lower temperatures than the nearby ordinary quantum Hall minima similar to the data reported in Ref. 11. This indicates that the related gaps in the energy spectrum are smaller than the Landau gap $\hbar\omega_c$. This gap is related to the spin-gap of spin-resolved Landau levels (see below). Data taken for different orientations of the Hall geometry with respect to the crystal axes are very similar excluding anisotropies of the underlying crystal lattice to be the origin for the observed phenomena. Within experimental resolution no hysteretic behavior in magnetic field and gate voltage was observed.

The data presented in Fig. 4(e) and the detail in Fig. 4(f) are generally similar to the results of Refs. 10 and 11. We interpret a dip in the magnetoresistance as being related to a gap in the energy spectrum of the system. The general strength of the observed features increases with magnetic field and density (mobility). In a single-particle picture the lowest density at which the features presented in Fig. 4(e) occur corresponds to the crossing points of the lowest Landau level of the upper subband with respective Landau levels in the lower subband. The total density can not be made large enough to observe the crossing points of the second Landau level in the upper subband with Landau levels in the lower subband. The lowest magnetic field, at which the features in Fig. 4(e) can be detected generally coincides with the beginning observation of spin splitting in the lowest subband. We would like to note, however, that weak precursors of such features can also be observed at relatively low magnetic fields where spin splitting cannot yet be resolved (see. Fig. 3). In this case there are no additional zeros in ρ_{xx}.

In the framework of filling factors related to the total carrier density $N_s^{tot}=N_s^{(1)}+N_s^{(2)}$ indicated by the dashed lines in Fig. 4(e) there is one dark feature (i.e., maximum) crossing a magnetoresistance minimum for odd filling factors. In contrast there are two dark features (maxima) for even filling factors delineating the ring-like structures described in Refs. 10 and 11.

A qualitative picture emerges by considering Landau level crossings as schematically indicated in Fig. 4(a). We label individual levels by (i,n,s), i.e., the subband quantum number $i=1,2$, the Landau-level quantum number $n=0,1,2,\ldots$, and the spin quantum number $s=\pm1/2$. The four involved Landau-levels are $(1,2,+)$ and $(1,2,-)$ with energies $E_{1,2,\pm}=5\hbar\omega_c/2\pm g^*\mu_BB$ and $(2,0,+)$ and $(2,0,-)$ with energy $E_\pm=\Delta E+\hbar\omega_c/2\pm g^*\mu_BB$. Here we have introduced the subband-separation in energy, ΔE, $\omega_c=eB/m^*$ is the cyclotron frequency, μ_B the Bohr-magneton, and g^* the effective Landé-factor. The crossing region of these four energy levels corresponds to the experimentally observed region encircled in Fig. 4(e).

In order to compare to the experiment, a crucial step is to translate the Landau-fan in the energy-magnetic field plane [Fig. 4(a)] to the experimentally relevant plane spanned by N_s^{tot} and magnetic field as shown in Fig. 4(b). This is a highly nonlinear mapping. We achieve this mapping by assuming Gaussian broadened Landau levels of width Γ. In transport experiments a peak in ρ_{xx} is expected when the Fermi energy lies in extended states near the density of state peak of a

Landau level. In Fig. 4(b) we therefore color regions corresponding to a band of 30 μeV around density of states maxima. This (arbitrary) choice of threshold was checked not to modify the results on a qualitative level.

While in the Landau-fan [Fig. 4(a)] the spacing between spin-split levels is typically different from the spacing of different Landau levels, in the N_s^{tot} representation all density of states peaks (and therefore maxima in ρ_{xx}) are equally spaced, if the Landau level separation is much larger than Γ, because each Landau level can maximally be occupied by eB/h electrons per area. If the Landau level separation in energy is comparable to their width, an uneven separation results. Therefore, for narrow Landau levels and far away from degeneracy points, peaks of the density of states are found at densities $N_s^{tot} = eB/h(p+1/2)$ with integer numbers p counting the number of completely filled Landau levels below the one considered [see. Fig. 4(b)]. In contrast, at magnetic fields where Landau-levels of the two subbands cross (points I–IV), peaks in the density of states are found at $N_s^{tot} = qeB/h$ with integer numbers q, i.e., exactly in the middle between the lines formed by the nondegenerate states. This argument intuitively explains the behavior of the four Landau levels presented in Fig. 4(a) when translated into the N_s^{tot}-B plane [Fig. 4(b)]. Crossing points I-IV between the four levels occur at the same magnetic field values in Figs. 4(a) and 4(b). We assign the same crossing points to the measured data in Fig. 4(f) which is a zoom into the region encircled in Fig. 4(e).

In the data presented in Fig. 4(f) we find slightly uneven spacing between the four levels at a given magnetic field far from the degeneracy points (e.g., at 2.8 T) indicating that the Landau-level width is only slightly smaller than the Zeeman splitting. From crossing points II and IV we determine the subband separation $\Delta E = 2\hbar\omega_c = 11.7$ meV for point II and 10.5 meV for point IV. We conclude that the subband spacing in the experiment depends on the total density, a finding which is in agreement with self-consistent calculations of parabolic (and also hard-wall) quantum wells.[14] From crossing points I and III we estimate $g^* = \Delta E/2\mu_B(1/B_I - 1/B_{III}) = 2.1$, a value which is enhanced over the bulk value presumably due to exchange effects.[19]

Stimulated by the above findings we extended the simple Landau-fan model presented above by including a linearly density-dependent subband separation $\Delta E(N_s^{tot})$ and the experimentally determined enhanced $g^* = 2.1$ in Fig. 4(c). It is remarkable that the emerging ringlike feature around 3.2 T resembles closely our data in Fig. 4(f) as well as the data in Fig. 2 of Ref. 11 in a single-particle picture, empirically extended by the density-dependent subband separation and the enhanced g^*.

Even better agreement with our data in Fig. 4(f) is achieved in Fig. 4(d) where we allow for a subband dependent Landau-level broadening Γ_i. The value of Γ_1 was estimated from low-field SdH oscillations where we find $\hbar/\tau_q = 240$ μeV. The value of Γ_2 was chosen in order to reproduce the experimentally observed motion of the resistivity peaks shown in Fig. 4(f). A more detailed calculation should replace the empirical inclusion of $\Delta E(N_s^{tot})$ by a self-consistent treatment and the empirically enhanced g^* by the
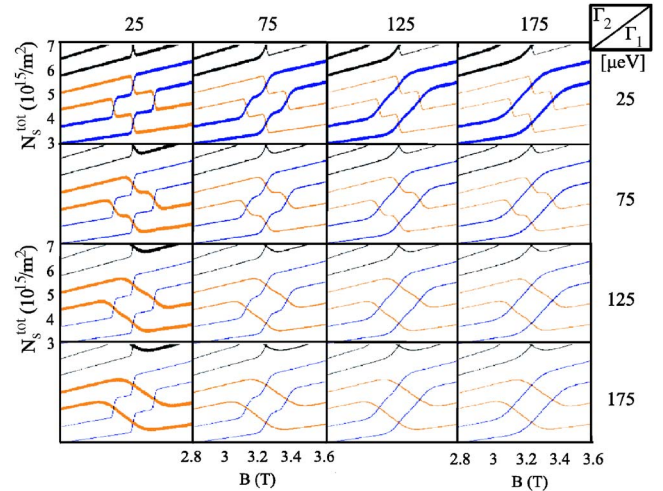

FIG. 6. (Color online) Simulated subband crossings to show the influence of different Landau level broadenings in the two involved subbands. The parameters used: g factor $g_{1,2^*} = 2$, a cutoff band of 5 μeV, and subband separation $\Delta E = 11$ meV.

calculated magnetic field dependent quantity for both subbands.[19] The subband density and with it the band structure will then become magnetic field dependent as observed in the data in the lower inset of Fig. 3. Possible interaction effects as discussed in Refs. 7 and 20 beyond those included above may further modify the details of the density of states.

The effective single-particle model contains parameters which are not exactly known from the experimental data, such as the broadening of the Landau levels belonging to the two subbands as well as the effective g factor, which can also be different for the two subbands. In order to show the variety of features which can be obtained with this model with a reasonable range of parameters we present in Fig. 6 a set of crossing situations similar to the regime depicted in Fig. 4(f). The parameters stepped along the vertical and horizontal axes in Fig. 6 are the Landau level widths $\Gamma_{1,2}$ of the two subbands. If the broadenings are the same, $\Gamma_1 = \Gamma_2$, i.e., one follows the diagonal form the upper left to the lower right, the crossing regime evolves from an ellipse-type structure (upper left) to a more quadrangle-type structure (lower right). If the two broadenings are very different then the crossover regime is characterized by a smooth variation of the Landau level with the larger broadening and a more rugged structure of the narrower Landau level (see lower left and upper right). A similar plot can be composed if one allows for different g factors in the two subbands. We conclude from these phenomenological calculations that a wide variety of Landau level crossing situations can be realized within a range of reasonable parameters pertinent to this effective single-particle model.

In conclusion, we have observed features in the magnetoresistance and Hall resistance of a two-subband system in a parabolic quantum well. The additional minima in ρ_{xx} are remarkably pronounced, non-hysteretic and reproducible. We demonstrate that the dominant features of the experimental data can be explained by a single-particle model empirically extended by an enhanced g^* and a density-dependent subband separation. Evidence for interaction effects beyond this

mean field Hartree and exchange approach cannot be reliably extracted from our data leaving this topic a challenge for future experiments.

---

*Permanent address: Department of Physics and Astronomy, Ohio University, Athens, Ohio 45701-2979, USA.

[1] R. E. Prange and S. M. Girvin, *The Quantum Hall effect*, 2nd ed. (Springer, New York, 1990).

[2] K. Muraki, T. Saku, Y. Hirayama, N. Kumada, A. Sawada, and Z. F. Ezawa, Solid State Commun. **112**, 625 (1999).

[3] N. Kumada, A. Sawada, Z. F. Ezawa, S. Nagahama, H. Azuhata, K. Muraki, T. Saku, and Y. Hirayama, J. Phys. Soc. Jpn. **69**, 3178 (2000).

[4] J. Eom, H. Cho, W. Kang, K. L. Campman, A. C. Gossard, T. Bichler, and W. Wegscheider, Science **289**, 2320 (2000).

[5] E. P. De Poortere, E. Tutuc, S. J. Papadakis, and M. Shayegan, Science **290**, 1546 (2000).

[6] T. Jungwirth and A. H. MacDonald, Phys. Rev. Lett. **87**, 216801 (2001).

[7] T. Jungwirth and A. H. MacDonald, Phys. Rev. B **63**, 035305 (2001).

[8] S. M. Girvin, Phys. Today **53**, 39 (2000).

[9] K. Muraki, T. Saku, and Y. Hirayama, Phys. Rev. Lett. **87**, 196801 (2001).

[10] A. G. Davies, C. H. W. Barnes, K. R. Zolleis, J. T. Nicholls, M. Y. Simmons, and D. A. Ritchie, Phys. Rev. B **54**, R17331 (1996).

[11] X. C. Zhang, D. R. Faulhaber, and H. W. Jiang, Phys. Rev. Lett. **95**, 216801 (2005).

[12] S. Lindemann, T. Ihn, T. Heinzel, W. Zwerger, K. Ensslin, K. Maranowski, and A. C. Gossard, Phys. Rev. B **66**, 195314 (2002).

[13] K. Ensslin, M. Sundaram, A. Wixforth, J. H. English, and A. C. Gossard, Phys. Rev. B **43**, 9988 (1991).

[14] K. Ensslin, A. Wixforth, M. Sundaram, P. F. Hopkins, J. H. English, and A. C. Gossard, Phys. Rev. B **47**, 1366 (1993).

[15] G. Salis, B. Graf, K. Ensslin, K. Campman, K. Maranowski, and A. C. Gossard, Phys. Rev. Lett. **79**, 5106 (1997).

[16] G. Salis, Y. Kato, K. Ensslin, D. C. Driscoll, A. C. Gossard, and D. D. Awschalom, Nature (London) **414**, 619 (2001).

[17] A. M. Chang and D. C. Tsui, Solid State Commun. **56**, 153 (1985).

[18] G. M. Gusev, A. A. Quivy, T. E. Lamas, J. R. Leite, O. Estibals, and J. C. Portal, Phys. Rev. B **67**, 155313 (2003).

[19] T. Ando, A. B. Fowler, and F. Stern, Rev. Mod. Phys. **54**, 437 (1982).

[20] D.-W. Wang, E. Demler, and S. Das Sarma, Phys. Rev. B **68**, 165303 (2003).